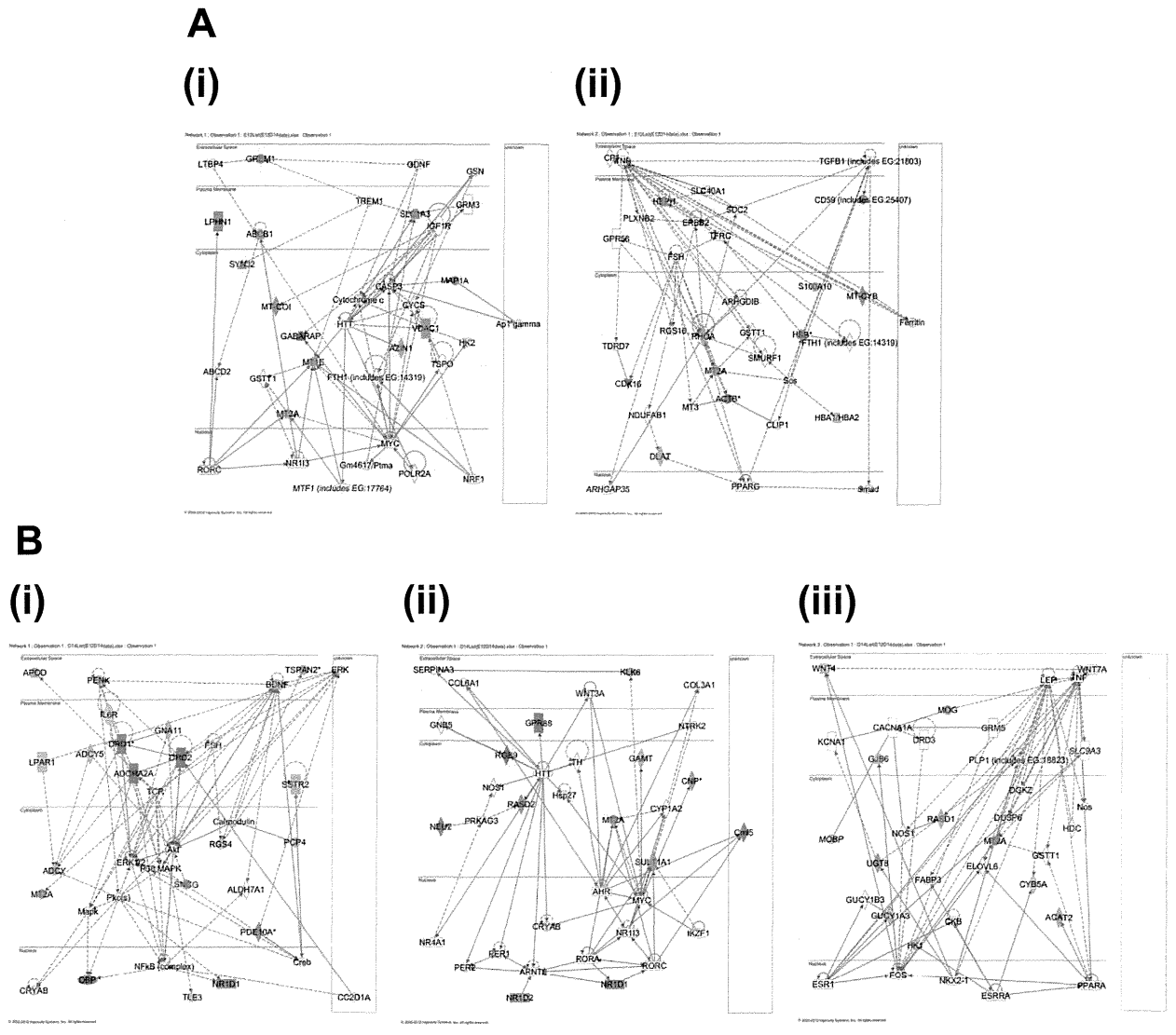

Fig. 5. IPA networks generated with significantly changed genes of E12IP and P14SC. A. The first (i) and second (ii) most significantly altered networks in E12IP. The most significantly changed network linked 'cell death', 'cellular compromise', and 'neurological disease'. The second most significantly changed network linked 'cell death', 'neurological disease', and 'carbohydrate metabolism'. B. The first (i), second (ii), and third (iii) most significantly changed networks in P14SC. These networks are related to 'nucleic acid metabolism' (i), 'cell signaling' (ii), and 'neurological disease' (iii).

[ii]), and 'neurological disease' (Fig. 5B [iii]). One notable aspect of these networks that was not observed in the E12IP networks is the alterations in the expression levels of nuclear genes such as DBP (transcription regulator), NR1D1 (nuclear receptor), and NR1D2 (nuclear receptor).

In conclusion, there are little similarities in the gene expression profiles between the two rat models for autism and regressive autism produced by pre- and post-natal exposures to VPA respectively. It is considered that that gene expression changes per se in the amygdala may be an important cause for impaired social behavior and enhanced anxiety, rather than expression changes of particular genes.

Table 1. The list of genes which changed significantly in E12IP

ID	Symbol	Entrez Gene name	Type(s)
Increase			
1389956_a_at	MT-COI	cytochrome c oxidase subunit I	enzyme
1367996_a_at	LPHN1	latrophilin 1	G-protein coupled receptor
1367882_at	MAP1A	microtubule-associated protein 1A	other
1388159_at	MT-CYB	cytochrome b	enzyme
1367929_at	CD59 (includes EG:25407)	CD59 molecule, complement regulatory protein	other
1398836_s_at	ACTB	actin, beta	other
1368127_at	NEU2	sialidase 2 (cytosolic sialidase)	enzyme
1398835_at	ACTB	actin, beta	other
1370326_at	CDK16	cyclin-dependent kinase 16	kinase
1370804_at	GABARAP	GABA(A) receptor-associated protein	transporter
1367593_at	SEPW1	selenoprotein W, 1	enzyme
1368554_at	PNLIP	pancreatic lipase	enzyme
1370459_at	C8orf85	chromosome 8 open reading frame 85	other
Decrease			
1387197_at	OMD	osteomodulin	other
1371245_a_at	HBB	hemoglobin, beta	transporter
1371130_at	SLC1A3	solute carrier family 1 (glial high affinity glutamate transporter), member 3	transporter
1368971_a_at	SYNJ2	synaptojanin 2	phosphatase
1371102_x_at	LOC100134871	beta globin minor gene	other
1369113_at	GREM1	gremlin 1	other
1371237_a_at	MT1E	metallothionein 1E	other
1368533_at	HEPH	hephaestin	transporter
1368588_at	DDX52	DEAD (Asp-Glu-Ala-Asp) box polypeptide 52	enzyme
1367771_at	Tsc22d3	TSC22 domain family, member 3	other
1386909_a_at	VDAC1	voltage-dependent anion channel 1	ion channel
1388271_at	MT2A	metallothionein 2A	other
1370464_at	ABCB1	ATP-binding cassette, sub-family B (MDR/TAP), member 1	transporter
1367553_x_at	HBB	hemoglobin, beta	transporter
1386890_at	S100A10	S100 calcium binding protein A10	other
1370575_a_at	AZIN1	antizyme inhibitor 1	enzyme
1370130_at	RHOA	ras homolog gene family, member A	enzyme
1388194_at	DLAT	dihydrolipoamide S-acetyltransferase	enzyme
1388608_x_at	HBA1/HBA2	hemoglobin, alpha 1	transporter

ID, symbol, entrez gene name, type of each gene were shown based on IPA software database.

Table 2. The list of genes which changed significantly in P14SC

ID	Symbol	Entrez Gene name	Type(s)
Increase			
1386904_a_at	CYB5A	cytochrome b5 type A (microsomal)	enzyme
1387897_at	CNP	2',3'-cyclic nucleotide 3' phosphodiesterase	enzyme
1370048_at	LPAR1	lysophosphatidic acid receptor 1	G-protein coupled receptor
1368092_at	FAH	fumarylacetoacetate hydrolase (fumarylacetoacetase)	enzyme
1368506_at	RGS4	regulator of G-protein signaling 4	other
1368298_at	ADCY5	adenylate cyclase 5	enzyme
1370834_at	HS3ST1	heparan sulfate (glucosamine) 3-O-sulfotransferase 1	enzyme
1368154_at	GUCY1A3	guanylate cyclase 1, soluble, alpha 3	enzyme
1368145_at	PCP4	Purkinje cell protein 4	other
1368253_at	GAMT	guanidinoacetate N-methyltransferase	enzyme
1387822_at	GNA11	guanine nucleotide binding protein (G protein), alpha 11 (Gq class)	enzyme
1368263_a_at	MOBP	myelin-associated oligodendrocyte basic protein	other
1367949_at	PENK	proenkephalin	other
1370206_at	ACCN4	amiloride-sensitive cation channel 4, pituitary	ion channel
1386979_at	SERINC5	serine incorporator 5	transporter
1368104_at	TSPAN2	tetraspanin 2	other
1372462_at	ACAT2	acetyl-CoA acetyltransferase 2	enzyme
1398257_at	MOG	myelin oligodendrocyte glycoprotein	other
1398258_at	APOD	apolipoprotein D	transporter
1368105_at	TSPAN2	tetraspanin 2	other
1368384_at	KLK6	kallikrein-related peptidase 6	peptidase
1370541_at	NR1D2	nuclear receptor subfamily 1, group D, member 2	ligand-dependent nuclear receptor
1370693_a_at	CNP	2',3'-cyclic nucleotide 3' phosphodiesterase	enzyme
1368121_at	AKR7A3	aldo-keto reductase family 7, member A3 (aflatoxin aldehyde reductase)	enzyme
1368438_at	PDE10A	phosphodiesterase 10A	enzyme
1368858_at	UGT8	UDP glycosyltransferase 8	enzyme
1370372_at	RASD2	RASD family, member 2	enzyme
1370816_at	NR1D1	nuclear receptor subfamily 1, group D, member 1	ligand-dependent nuclear receptor
1368478_at	DRD1	dopamine receptor D1	G-protein coupled receptor
1370669_a_at	PDE10A	phosphodiesterase 10A	enzyme
1387874_at	DBP	D site of albumin promoter (albumin D-box) binding protein	transcription regulator
1388176_at	Cml5	camello-like 5	enzyme
1368135_at	NINJ2	ninjurin 2	other
1368127_at	NEU2	sialidase 2 (cytosolic sialidase)	enzyme
1368479_at	DRD1	dopamine receptor D1	G-protein coupled receptor

Table 2. (Continued)

ID	Symbol	Entrez Gene name	Type(s)
Increase			
1387241_at	GPR88	G protein-coupled receptor 88	G-protein coupled receptor
1368708_a_at	DRD2	dopamine receptor D2	G-protein coupled receptor
1368300_at	ADPRA2A	adenosine A2a receptor	G-protein coupled receptor
1368500_a_at	RGS9	regulator of G-protein signaling 9	enzyme
1370991_at	Cml3/Gm4477	camello-like 3	enzyme
Decrease			
1370550_at	LSAMP	limbic system-associated membrane protein	other
1370026_at	CRYAB	crystallin, alpha B	other
1386987_at	IL6R	interleukin 6 receptor	transmembrane receptor
1368641_at	WNT4	wingless-like MMTV integration site family, member 4	cytokine
1387169_at	TLE3	transducin-like enhancer of split 3 (E(sp 1) homolog, Drosophila)	other
1368577_at	GJB6	gap junction protein, beta 6, 30kDa	transporter
1386929_at	HK1	hexokinase 1	kinase
1368782_at	SSTR2	somatostatin receptor 2	G-proein coupled receptor
1368677_at	BDNF	brain-derived neurotrophic factor	growth factor
1387908_at	RASD1	RAS, dexamethasone-induced 1	enzyme
1370019_at	SULT1A1	sulfotransferase family, cytosolic, 1A, phenol-preferring, member 1	enzyme
1398245_at	SNCG	synuclein, gamma (breast cancer-specific protein 1)	other
1388271_at	MT2A	metallothionein 2A	other

ID, symbol, entrez gene name, type of each gene were shown based on IPA software database.

Table 3. The list of genes which changed significantly in E12IP and P14SC were categorized to groups based on their functions using IPA software

E12IP			P14SC	
p-value	Molecules	Category	P14SC	p-value
		Behavior	RGS9,GJB6,RASD2,DBP,BDNF,PDE10A,IL6R,CNP,SNCG,DRD2,PCP4,DRD1,NR1D1,LPAR1,ADCY5,PENK,ADORA2A	2.16E-07-1.85E-02
1.02E-02-1.02E-02	RHOA	Cell Cycle	CRYAB,SSTR2,WNT4	4.65E-03-1.85E-02
6.33E-06-3.04E-02	ABCB1,CD59,MT2A,RHOA,ACTB,GREM1,VDAC1,MT1E	Cell Death	CRYAB,BDNF,IL6R,RGS4,UGT8,DRD2,HK1,LPAR1,SSTR2,ADCY5,MT2A,ADORA2A,MOG	3.03E-04-2.31E-02
2.56E-03-4.46E-02	CD59,HBB,MT2A,RHOA,SLC1A3,VDAC1	Cell Morphology	HK1,LPAR1,DRD1,MT2A,BDNF,IL6R,GNA11,KLK6,RGS4,SNCG,DRD2,ADORA2A	4.59E-04-2.31E-02
4.93E-02-4.93E-02	CD59,HBA1/HBA2,VDAC1	Cell Signaling	RGS9,LPAR1,SSTR2,DRD1,BDNF,ADCY5,PDE10A,IL6R,GNA11,RGS4,DRD2,ADORA2A	9.12E-05-2.07E-02
6.3E-05-2.54E-02	CD59,MT2A,RHOA,SLC1A3,GREM1,GABARAP,VDAC1,LPHN1,MT1E,S100A10	Cell-To-Cell Signaling and Interaction	RASD2,GUCY1A3,BDNF,GNA11,CNP,IL6R,RGS4,KLK6,SNCG,DRD2,PCP4,DRD1,ADCY5,MT2A,SULT1A1,PENK,ADORA2A,MOG,NINJ2	2.34E-07-2.31E-02
6.33E-06-4.27E-02	SYNJ2,CD59,MT2A,RHOA,HBA1/HBA2,VDAC1,LPHN1,MT1E	Cellular Assembly and Organization	RGS9,HK1,CRYAB,LPAR1,DRD1,MT2A,BDNF,GNA11,CNP,SNCG,DRD2,MOG	4.65E-03-2.31E-02
4.67E-04-4.46E-02	Tsc22d3,HBB,MT2A,RHOA,HBA1/HBA2,SLC1A3,	Cellular Development	NR1D1,DRD1,MT2A,BDNF,SERINC5,IL6R,RGS4,UGT8,DRD2	5.55E-04-2.31E-02
1.32E-04-4.27E-02	CD59,MT2A,RHOA,HBA1/HBA2,VDAC1,LPHN1,MT1E	Cellular Function and Maintenance	CRYAB,DRD1,BDNF,CNP	4.65E-03-2.31E-02
4.67E-04-2.07E-02	ABCB1,MT2A,RHOA,ACTB,GREM1,GABARAP,VDAC1,MT1E	Cellular Growth and Proliferation	GJB6,CRYAB,GUCY1A3,BDNF,IL6R,GNA11,KLK6,RGS4,SNCG,DRD2,RASD1,SSTR2,LPAR1,NR1D1,MT2A,PENK,WNT4,ADORA2A,MOG	3.03E-04-2.17E-02
2.56E-03-4.77E-02	CD59,RHOA,LPHN1,S100A10	Cellular Movement	GUCY1A3,BDNF,GNA11,CNP,IL6R,RGS4,KLK6,SNCG,DRD2,NR1D1,SSTR2,DRD1,LPAR1,PENK,ADORA2A,MOG	6.76E-05-1.85E-02
1.67E-05-2.54E-02	Tsc22d3,MT2A,RHOA,GREM1,VDAC1,MT1E	Connective Tissue Development and Function		
5.12E-03-4.27E-02	HBB,RHOA,PNLIP	Developmental Disorder	CRYAB,GJB6,SSTR2,DRD1,GUCY1A3,BDNF,IL6R,GNA11,WNT4,RGS4,DRD2	2.02E-05-2.31E-02
7.67E-03-7.67E-03	ABCB1	DNA Replication, Recombination, and Repair	GUCY1A3,BDNF,RGS4,DRD2,ADORA2A	1.28E-02-1.28E-02
2.56E-03-4.27E-02	ABCB1	Drug Metabolism	DRD1,BDNF,SULT1A1,GNA11,RGS4,SNCG,DRD2,ADORA2A	2.12E-05-1.85E-02
2.56E-03-4.77E-02	HBB,RHOA,GREM1	Embryonic Development	GJB6,LPAR1,BDNF,WNT4,KLK6,DRD2	1.17E-03-1.85E-02
2.56E-03-2.56E-03	ABCB1	Endocrine System Development and Function	BDNF,SULT1A1,GNA11,WNT4,ADORA2A	2.1E-04-2.31E-02
2.25E-02-2.25E-02	MT1E,S100A10	Endocrine System Disorders	ACAT2,SSTR2,DRD1,IL6R,DRD2	2.02E-05-2.31E-02
4.52E-02-4.52E-02	RHOA	Gene Expression	DBP,BDNF,IL6R,RGS4,KLK6,NR1D2,DRD2,RASD1,NR1D1,DRD1,LPAR1,TLE3,WNT4,ADORA2A,MOG	1.38E-02-1.39E-02

Table 3. (Continued)

E12IP			P14SC	
p-value	Molecules	Category	P14SC	p-value
1.29E-03-4.27E-02	ABCB1,HBB,MT2A,ACTB,PNLIP,MT1E	Genetic Disorder	ACCN4,RGS9,CRYAB,GJB6,RASD2,ACAT2,BDNF,GNA11,KLK6,NR1D2,DRD1,ADCY5,MT2A,WNT4,LSAMP,MOG,GUCY1A3,DBP,PDE10A,CNP,IL6R,TSPAN2,RGS4,NEU2,SNCG,DRD2,GPR88,FAH,PCP4,LPAR1,NR1D1,MOBP,SSTR2,SULT1A1,PENK,TLE3,CYB5A,ADORA2A,APOD	4.1E-09-2.31E-02
2.56E-03-4.27E-02	ABCB1,RHOA,MT1E	Inflammatory Disease	CRYAB,BDNF,IL6R,DRD2,MOG	4.65E-03-2.31E-02
2.56E-03-4.27E-02	CD59,RHOA,MT1E,S100A10	Inflammatory Response	GNA11,IL6R,PENK,CNP,ADORA2A,MOG	9.29E-03-2.31E-02
2.56E-03-4.4E-02	SYNJ2,ABCB1,MT2A,DLAT,RHOA,MT1E,PNLIP,S100A10	Lipid Metabolism	ACAT2,DBP,BDNF,SERINC5,GNA11,RGS4,UGT8,DRD2,LPAR1,DRD1,SSTR2,SULT1A1,WNT4,ADORA2A,MOG,APOD	2.1E-04-2.31E-02
6.33E-06-4.93E-02	ABCB1,CD59,HBA1/HBA2,CDK16,SLC1A3,HEPH,LPHN1,HBB,MT-CYB,MT2A,RHOA,GABARAP,VDAC1,MT1E,PNLIP,S100A10	Molecular Transport	ACAT2,GUCY1A3,BDNF,PDE10A,GNA11,IL6R,RGS4,UGT8,SNCG,DRD2,HK1,LPAR1,SSTR2,DRD1,MT2A,ADCY5,WNT4,ADORA2A,APOD	1.11E-05-2.31E-02
3.99E-03-4.27E-02	MT2A,RHOA,HBA1/HBA2,SLC1A3,GABARAP,VDAC1,LPHN1,MT1E	Nervous System Development and Function	GJB6,RASD2,GUCY1A3,DBP,BDNF,SERINC5,CNP,GNA11,RGS4,UGT8,SNCG,DRD2,PCP4,DRD1,NR1D1,LPAR1,ADCY5,MT2A,PENK,ADORA2A,MOG,NINJ2	1.59E-05-2.31E-02
3.79E-05-3.78E-02	MT2A,ACTB,SLC1A3,MT1E,S100A10	Neurological Disease	RGS9,CRYAB,RASD2,GJB6,BDNF,GNA11,DRD1,MT2A,ADCY5,LSAMP,MOG,GUCY1A3,DBP,PDE10A,CNP,IL6R,RGS4,SNCG,DRD2,GPR88,PCP4,LPAR1,MOBP,SSTR2,NR1D1,PENK,ADORA2A,APOD	1.43E-09-2.31E-02
2.64E-02-2.64E-02	MT2A,MT1E	Psychological Disorders	CRYAB,BDNF,PDE10A,CNP,RGS4,DRD2,PCP4,MOBP,DRD1,SSTR2,MT2A,LSAMP,ADORA2A,MOG,APOD	1.57E-04-2.01E-02
6.33E-06-4.4E-02	ABCB1,AZIN1,HBA1/HBA2,SLC1A3,SYNJ2,HBB,MT2A,RHOA,DLAT,VDAC1,PNLIP,MT1E,S100A10	Small Molecule Biochemistry	RGS9,ACAT2,BDNF,SERINC5,GNA11,HK1,DRD1,MT2A,ADCY5,WNT4,MOG,DBP,GUCY1A3,PDE10A,IL6R,RGS4,UGT8,SNCG,DRD2,SSTR2,LPAR1,GAMT,SULT1A1,CYB5A,ADORA2A,APOD	1.11E-05-2.31E-02
2.56E-03-2.79E-02	CD59,Tsc22d3,HBB,RHOA,SLC1A3,GREM1	Tissue Development	GJB6,CRYAB,GUCY1A3,BDNF,GNA11,CNP,IL6R,KLK6,RGS4,DRD2,GAMT,DRD1,LPAR1,TLE3,WNT4,ADORA2A,MOG,NINJ2	4.59E-04-2.31E-02
3.43E-04-2.79E-02	CD59,HBB,MT2A,RHOA,SLC1A3,GREM1,MT1E,S100A10	Tissue Morphology	CRYAB,ACAT2,GUCY1A3,BDNF,IL6R,DRD2,GAMT,DRD1,SSTR2,LPAR1,WNT4,ADORA2A,MOG	8E-04-2.31E-02

Behavior'-related genes were identified only in P14SC. Additionally a larger number of genes were categorized to 'nervous system development and function', 'neurological disease', and 'psychological disorders' in P14SC than in E12IP.

ACKNOWLEDGMENT

This work was supported by Grants-in-Aid from the Food Safety Commission of Japan (No. 1003).

REFERENCES

Blackford, J.U. and Pine, D.S. (2012): Neural substrates of childhood anxiety disorders: a review of neuroimaging findings. Child Adolesc. Psychiatr. Clin. N. Am., **21**, 501-525.

Etkin, A. and Wager, T.D. (2007): Functional neuroimaging of anxiety: a meta-analysis of emotional processing in PTSD, social anxiety disorder, and specific phobia. Am. J. Psychiatry., **164**, 1476-1488.

Markram, K., Rinaldi, T., Mendola, D.L., Sandi, C. and Markram, H. (2008): Abnormal fear conditioning and amygdala processing in an animal model of autism. Neuropsychopharmacology, **33**, 901-912.

Neuhaus, E., Beauchaine, T.P. and Bernier, R. (2010): Neurobiological correlates of social functioning in autism. Clin. Psychol. Rev., **30**, 733-748.

Schneider, T. and Przewtocki, R. (2005): Behavioral alterations in rats prenatally exposed to valproic acid: Animal model of autism. Neuropsychopharmacology, **30**, 80-89.

Schneider, T., Ziolkowska, T., Gieryk, T., Tyminska, T. and Przewlocki, R. (2007): Prenatal exposure to valproic acid disturbs the enkephalinergic system functioning, basal hedonic tone, and emotional responses in an animal model of autism. Psychopharmacology, **193**, 547-555.

Schneider, T., Roman, A., Basta-Kaim, A., Kubera, M., Budziszewska, B., Schneider, K. and Przewtochi, R. (2008): Gender-specific behavioral and immunological alterations in an animal model of autism induced by prenatal exposure to valproic acid. Psychoneuroendocrinology, **33**, 728-740.

Wagner, G.C., Reuhl, K.R., Cheh, M., McRae, P. and Halladay, A.K. (2006): A new neurobehavioral model of autism in mice: Pre- and postnatal exposure to sodium valproate. J Autism Dev. Disord., **36**, 779-793.

Yochum, C.L., Dowling, P., Reuhl, K.R., Wagner, G.C. and Ming, X. (2008): VPA-induced apoptosis and behavioral deficits in neonatal mice. Brain Res., **1203**, 126-132.

Yochum, C.L., Bhattacharya, P., Patti, L., Mirochnitchenko, L. and Wagner, G.C. (2010): Animal model of autism using GSTM1 knockout mice and early post-natal sodium valproate treatment. Behav. Brain Res., **210**, 202-210.

Metallomics

RSC Publishing

PAPER

View Article Online
View Journal | View Issue

AMP-activated protein kinase-mediated glucose transport as a novel target of tributyltin in human embryonic carcinoma cells†

Cite this: *Metallomics*, 2013, **5**, 484

Shigeru Yamada,[a] Yaichiro Kotake,[b] Yuko Sekino[a] and Yasunari Kanda*[a]

Organotin compounds such as tributyltin (TBT) are known to cause various forms of cytotoxicity, including developmental toxicity and neurotoxicity. However, the molecular target of the toxicity induced by nanomolar levels of TBT has not been identified. In the present study, we found that exposure to 100 nM TBT induced growth arrest in human pluripotent embryonic carcinoma cell line NT2/D1. Since glucose provides metabolic energy, we focused on the glycolytic system. We found that exposure to TBT reduced the levels of both glucose-6-phosphate and fructose-6-phosphate. To investigate the effect of TBT exposure on glycolysis, we examined glucose transporter (GLUT) activity. TBT exposure inhibited glucose uptake *via* a decrease in the level of cell surface-bound GLUT1. Furthermore, we examined the effect of AMP-activated protein kinase (AMPK), which is known to regulate glucose transport by facilitating GLUT translocation. Treatment with the potent AMPK activator, AICAR, restored the TBT-induced reduction in cell surface-bound GLUT1 and glucose uptake. In conclusion, these results suggest that exposure to nanomolar levels of TBT causes growth arrest by targeting glycolytic systems in human embryonic carcinoma cells. Thus, understanding the energy metabolism may provide new insights into the mechanisms of metal-induced cytotoxicity.

Received 28th December 2012,
Accepted 20th February 2013

DOI: 10.1039/c3mt20268b

www.rsc.org/metallomics

Introduction

Growing evidence suggests that environmental metals contribute to developmental toxicity and neurotoxicity.[1–3] Since the developing brain is inherently more vulnerable to injury than the adult brain, exposure to metals during early fetal development can potentially cause neurological disorders at doses much lower than those that are toxic in adults.[4–7] Therefore, it is necessary to elucidate the cytotoxic effects of such metals at low levels.

Organotin compounds are well known to cause cytotoxicity. Although organotin compounds or derivatives have been shown to have a potential anti-tumor activity[8,9] and some of them have already been entered into preclinical trials,[10] tributyltin (TBT) is considered to be associated with developmental toxicity and neurotoxicity.[11] For example, TBT can cause increased fetal mortality, decreased fetal birth weights, and behavioral abnormalities in rat offspring.[12,13] TBT is known to affect fertilization and embryonic development.[14] Moreover, TBT has been shown to induce neuronal death by glutamate excitotoxicity in cultured rat cortical neurons.[15] Although the use of TBT has already been restricted, butyltin compounds, including TBT, have been reported to be still present at concentrations between 50 and 400 nM in human blood.[16] However, the mechanism by which nanomolar levels of TBT cause cytotoxicity is not fully understood.

Glucose is the primary energy source for homeostasis. Glucose transport across the plasma membrane *via* a glucose transporter (GLUT) is a rate-limiting step in glucose metabolism.[17] AMP-activated protein kinase (AMPK), a serine threonine kinase, has been shown to regulate glucose uptake by facilitating the translocation of the GLUT to the membrane or by activation of transporter activity at the plasma membrane.[18,19] The fetal brain has been reported to rely on anaerobic glycolysis to meet its energy demands.[20] Thus, GLUT is considered essential in the early organogenesis period. GLUT1, a major subtype of GLUT in fetal tissue, has been shown to mediate organogenesis in rat embryos.[21] In addition, clinical data regarding human GLUT1 deficiency syndrome suggest that GLUT1 is necessary for human brain development.[22]

In the present study, we hypothesized a possible link between TBT toxicity and glucose metabolism. We found that

[a] *Division of Pharmacology, National Institute of Health Sciences, 1-18-1, Kamiyoga, Setagaya-ku 158-8501, Japan. E-mail: kanda@nihs.go.jp; Fax: +81-3-3700-9704; Tel: +81-3-3700-9704*

[b] *Department of Xenobiotic Metabolism and Molecular Toxicology, Graduate School of Biomedical and Health Sciences, Hiroshima University, Japan*

† Electronic supplementary information (ESI) available. See DOI: 10.1039/c3mt20268b

exposure to TBT reduced the amounts of glucose-6-phosphate and fructose-6-phosphate *via* a decrease in surface-bound GLUT1 in the human pluripotent embryonic carcinoma cell line NT2/D1. In addition, treatment with the potent AMPK activator, 5-aminoimidazole-4-carboxyamide ribonucleoside (AICAR), restored the inhibitory effect of TBT on both cell surface-bound GLUT1 levels and glucose uptake. We report here that the glycolytic pathway is a molecular target of nanomolar levels of TBT in human embryonic carcinoma cells.

Methods

Cell culture

NT2/D1 cells were obtained from the American Type Culture Collection. The cells were cultured in Dulbecco's modified Eagle's medium (DMEM; Sigma-Aldrich, St. Louis, MO, USA) supplemented with 10% fetal bovine serum (FBS; Biological Industries, Ashrat, Israel) and 0.05 mg mL^{-1} penicillin–streptomycin mixture (Life Technologies, Carlsbad, CA, USA) at 37 °C and 5% CO_2. For neural differentiation, all-trans retinoic acid (RA; Sigma-Aldrich) was added to the medium twice a week at a final concentration of 10 μM.

Cell proliferation assay

Cell viability was measured using the CellTiter 96 AQueous One Solution Cell Proliferation Assay (Promega, Madison, WI, USA), according to the manufacturer's instructions. Briefly, NT2/D1 cells were seeded into 96-well plates and exposed to different concentrations of TBT. After exposure to TBT, One Solution Reagent was added to each well, and the plate was incubated at 37 °C for another 2 h. Absorbance was measured at 490 nm using an iMark microplate reader (Bio-Rad, Hercules, CA, USA).

Glucose uptake assay

A glucose uptake assay was performed using a fluorescent glucose derivative, 2-[*N*-(7-nitrobenz-2-oxa-1,3-diazol-4-yl)amino]-2-deoxy-D-glucose (2-NBDG; Peptide Institute Inc., Osaka, Japan) by the previously reported procedure with slight modifications.[23] Briefly, NT2/D1 cells exposed to TBT were incubated with 2-NBDG (100 μM) for 2 h at 37 °C. The 2-NBDG uptake reaction was stopped by draining the incubation medium and washing the cells twice with ice-cold PBS. The incorporated 2-NBDG was measured using a Wallac1420ARVO fluoroscan (Perkin-Elmer, Waltham, MA, USA) with excitation at 488 nm and emission at 515 nm. The fluorescence intensities were normalized to the total protein content.

Hexokinase activity assay

Hexokinase activity was determined using a commercial Hexokinase Colorimetric Assay Kit (Biovision, Mountain View, CA, USA), according to the manufacturer's instructions.

AMPK activity assay

AMPK activity was determined using a commercial CycLex AMP Kinase Assay Kit (MBL International, Woburn, MA, USA), according to the manufacturer's instructions.

Determination of glucose-6-phosphate and fructose-6-phosphate

Intracellular metabolites were extracted and used for subsequent capillary electrophoresis time-of-flight mass spectrometry (CE-TOFMS) analysis, as described previously.[24] Glucose-6-phosphate and fructose-6-phosphate were determined using an Agilent CE capillary electrophoresis system (Agilent Technologies, Waldbronn, Germany) equipped with an Agilent G3250AA LC/MSD TOF system (Agilent Technologies, Palo Alto, CA), an Agilent 1100 series isocratic HPLC pump, a G1603A Agilent CE-MS adapter kit, and a G1607A Agilent CE-electrospray ionization 53-MS sprayer kit. For system control and data acquisition, G2201AA Agilent ChemStation software was used for CE, and Agilent TOF (Analyst QS) software was used for TOFMS.

Western blotting

Western blotting was performed as previously reported.[25] Briefly, the cells were lysed using Cell Lysis Buffer (Cell Signaling Technology, Danvers, MA, USA), and proteins were then separated by sodium dodecyl sulfate (SDS)-polyacrylamide gel electrophoresis and electrophoretically transferred to Immobilon-P membranes (Millipore, Billerica, MA, USA). The membranes were probed using primary antibodies (anti-GLUT1 polyclonal antibodies [1:200; Santa Cruz Biotechnology, Santa Cruz, CA, USA], anti-c-Myc polyclonal antibodies [1:1000; Sigma-Aldrich], anti-Flag monoclonal antibodies [1:1000; Sigma-Aldrich], and anti-β-actin monoclonal antibodies [1:1000; Sigma-Aldrich]). The membranes were then incubated with secondary antibodies against rabbit or mouse IgG conjugated with horseradish peroxidase (Cell Signaling Technology). The bands were visualized using an ECL Western Blotting Analysis System (GE Healthcare, Buckinghamshire, UK), and images were acquired using a LAS-3000 Imager (Fujifilm UK Ltd., Systems, Bedford, UK). The density of each band was quantified with ImageJ software (NIH, Bethesda, MD, USA).

Cell surface biotinylation

NT2/D1 cell surface proteins were biotinylated using a Cell Surface Protein Isolation Kit, according to the manufacturer's instructions (Pierce, Rockford, IL, USA). Briefly, cells were incubated with ice-cold phosphate-buffered saline (PBS; pH 7.4) containing Sulfo-NHS-SS-Biotin, with gentle rocking for 30 min at 4 °C. The biotinylated proteins were precipitated with streptavidin beads and eluted from the beads with SDS sample buffer. The proteins were analyzed by western blotting with anti-GLUT1 antibodies.

Immunohistochemistry

Cells, cultured on glass coverslips, were fixed in 4% paraformaldehyde in PBS (pH 7.4) for 15 min at room temperature. The fixed cells were incubated with anti-GLUT1 polyclonal antibodies (1:100; Santa Cruz) for 1 h at room temperature. Finally, they were incubated with Alexa488-conjugated secondary antibodies (1:200; Life Technologies) for 1 h at room temperature. The cells were enclosed in SlowFade (Life Technologies) and examined under a BIOREVO BZ-9000 fluorescent microscope (Keyence, Osaka, Japan).

Transfection

Cells were transiently transfected with Flag-tagged GLUT1 in pEF6 (a kind gift from Dr Rathmell) and c-Myc-tagged constitutively active-AMPK-α1 (T172D) or c-Myc-tagged dominant-negative-AMPK-α1 (K45R) in pcDNA3 (a kind gift from Dr Carling) using the FuGene HD Transfection Reagent (Promega), according to the manufacturer's protocol. After 48 h incubation, the transfectants were cultured with 12.5 μg mL^{-1} blasticidin or 0.5 mg mL^{-1} G418.

Real-time PCR

After total RNA was isolated from NT2/D1 cells using TRIzol (Life Technologies), quantitative real-time reverse transcription (RT)-PCR with a QuantiTect SYBR Green RT-PCR Kit (QIAGEN, Valencia, CA, USA) was performed using an ABI PRISM 7900HT sequence detection system (Applied Biosystems, Foster City, CA, USA), as previously reported.[26] The relative changes in the amounts of transcripts in each sample were normalized using ribosomal protein L13 (RPL13) mRNA levels. The sequences of the primers used for real-time PCR analysis are as follows: GLUT1 (forward, 5′-CCAGCTGCCATTGCCGTT-3′; reverse, 5′-GACGTAGGGACCACACAGTTGC-3′), GLUT2 (forward, 5′-CACACAAGACCTGGAATTGACA-3′; reverse, 5′-CGGTCATCCAGTGGAACAC-3′), GLUT3 (forward, 5′-CAATGCTCCTGAGAAGATCATAA-3′; reverse, 5′-AAAGCGGTTGACGAAGAGT-3′), GLUT4 (forward, 5′-CTGGGCCTCACAGTGCTAC-3′; reverse, 5′-GTCAGGCGCTTCAGACTCTT-3′), nestin (forward, 5′-GGCAGCGTTGGAACAGAGGT-3′; reverse, 5′-CATCTTGAGGTGCGCCAGCT-3′), NeuroD (forward, 5′-GGAAACGAACCCACTGTGCT-3′; reverse, 5′-GCCACACCAAATTCGTGGTG-3′), Math1 (forward, 5′-GTCCGAGCTGCTACAAACG-3′; reverse, 5′-GTGGTGGTGGTCGCTTTT-3′), MAP2 (forward, 5′-CCAATGGATTCCCATACAGG-3′; reverse, 5′-CTGCTACAGCCTCAGCAGTG-3′), RPL13 (forward, 5′-CATCGTGGCTAAACAGGTACTG-3′; reverse, 5′-GCACGACCTTGAGGGCAGCC-3′).

Materials

TBT was obtained from Tokyo Chemical Industry (Tokyo, Japan). Tin acetate (TA), AICAR, and rosiglitazone were obtained from Sigma-Aldrich. All other reagents were of analytical grade and obtained from commercial sources.

Statistical analysis

All data were presented as mean ± S.D. ANOVA followed by a *post hoc* Tukey test was used to analyze data in Fig. 1–4. Unpaired Student's *t* test was used to analyze data in Fig. 5. A *p* value of less than 0.05 was considered significant.

Results

To examine the effect of TBT on the proliferation of human NT2/D1 embryonic carcinoma cells, we exposed the cells to different concentrations of TBT for 24 h and measured cell viability by MTT assay. Treatment with TBT reduced cell viability in a dose-dependent manner (Fig. 1A; 0.03–0.3 μM). We observed that almost all cells were detached from the culture dish at TBT concentrations of 300 nM and above. In contrast, the less toxic TA had little effect at any concentration (Fig. 1A–e). We performed time-course experiments with 100 nM TBT, and determined the cell number. Exposure to

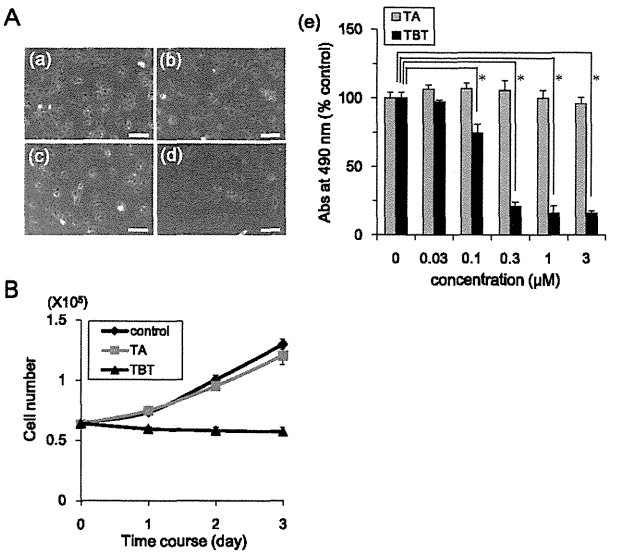

Fig. 1 Effect of TBT exposure on cell proliferation in NT2/D1 cells. (A) NT2/D1 cells were seeded into 96-well plates and exposed to TBT at different concentrations for 24 h. (a–d) Phase-contrast photomicrographs of NT2/D1 cells exposed to TBT at 0, 0.03, 0.1, or 0.3 μM (Bar = 100 μm). (e) Cell viability in the presence of TBT or TA was examined using the CellTiter 96 AQueous One Solution Cell Proliferation Assay. (B) NT2/D1 cells (6×10^5 cells) were seeded into 100 mm dishes and exposed to 100 nM TBT. After 24, 48, and 72 h, cell count was determined using a hemocytometer. *$P < 0.05$.

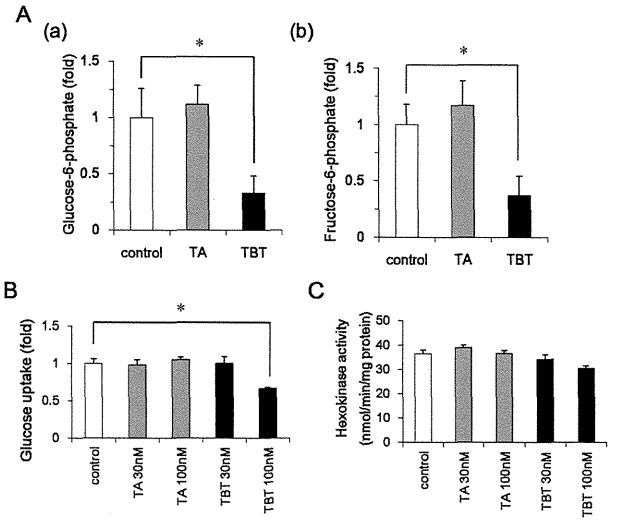

Fig. 2 Effect of TBT exposure on glycolytic systems in NT2/D1 cells. (A) After 24 h exposure to 100 nM TBT or TA, glucose 6-phosphate (a) and fructose 6-phosphate (b) levels were determined using CE-TOFMS. (B) After exposure to TBT or TA (30, 100 nM) for 24 h, glucose uptake assay was performed using a fluorescent glucose analog 2-NBDG. The fluorescence intensities of incorporated 2-NBDG were normalized to total cellular protein content. (C) After exposure to TBT or TA (30, 100 nM) for 24 h, hexokinase activity was measured using a commercial assay kit. *$P < 0.05$.

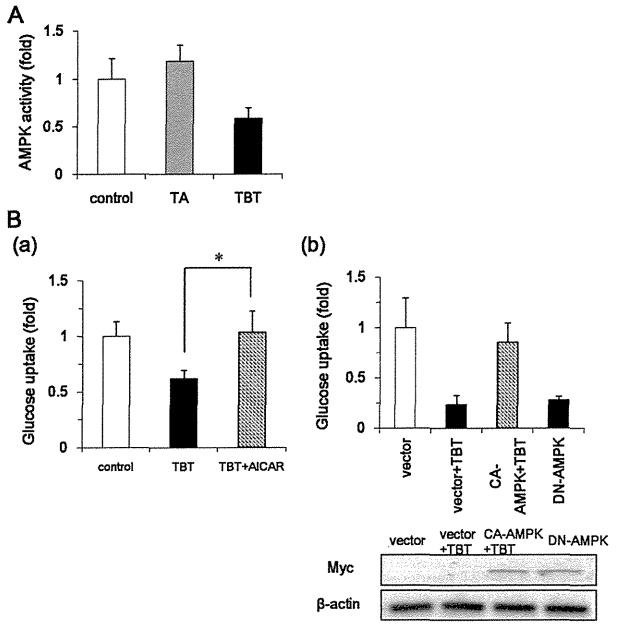

Fig. 3 Effect of AMPK on glucose uptake in NT2/D1 cells. (A) NT2/D1 cells were exposed to TBT or TA at 100 nM for 24 h. AICAR (0.5 mM) treatment was performed for 3 h. AMPK activity in the lysed cells was determined using a commercial assay kit. (B) NT2/D1 cells were exposed to TBT in the presence of 0.5 mM AICAR. (C) After overexpression of constitutively active (CA) mutants of AMPK, NT2/D1 cells were exposed to 100 nM TBT for 24 h, and glucose uptake assay was performed. After overexpression of dominant-negative (DN) mutants of AMPK, basal glucose uptake was tested. A glucose uptake assay was performed using the fluorescent glucose analog 2-NBDG. The fluorescence intensities of incorporated 2-NBDG were normalized to total cellular protein content. $^*P < 0.05$.

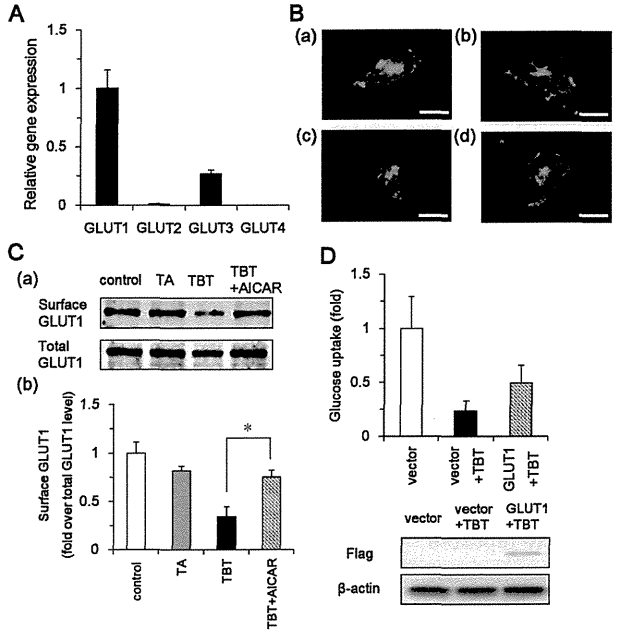

Fig. 4 Effect of TBT exposure on GLUT1 localization in NT2/D1 cells. (A) Expression of GLUT family by real-time PCR in NT2/D1 cells. Relative changes were determined by normalizing to RPL13. (B) After exposure to 100 nM TBT for 24 h, NT2/D1 cells were immunostained with anti-GLUT1 polyclonal antibodies. (a) Control, (b) 100 nM TA, (c) 100 nM TBT, and (d) 100 nM TBT + 0.5 mM AICAR. (Bar = 25 μm). (C) (a) NT2/D1 cell surface proteins were biotinylated using Sulfo-NHS-SS-Biotin, and then lysed. After precipitation with streptavidin beads, biotinylated proteins were analyzed by western blotting using anti-GLUT1 antibodies. Total GLUT1 protein was detected in cell lysate. (b) The relative density of bands was quantified with ImageJ software. Cell surface GLUT1 levels were normalized to total GLUT1 levels. (D) After overexpression of GLUT1, NT2/D1 cells were exposed to 100 nM TBT for 24 h, and glucose uptake assay was performed using the fluorescent glucose analog 2-NBDG. The fluorescence intensities of incorporated 2-NBDG were normalized to total cellular protein content. $^*P < 0.05$.

TBT suppressed the growth curve, but the total cell number did not alter throughout the time-course experiment (Fig. 1B). These data suggest that exposure to 100 nM TBT induced growth arrest in the cells without causing cell death.

Glucose provides metabolic energy for cell growth and it is incorporated by glucose transporters.[17] To examine the mechanism by which TBT induces growth arrest at low concentrations, we determined the glucose-6-phosphate, a major metabolite in glycolysis. We found that exposure to 100 nM TBT reduced the amount of glucose-6-phosphate (Fig. 2A). Fructose-6-phosphate, which is produced by isomerization of glucose 6-phosphate, also reduced by TBT. To check whether the decrease in glucose-6-phosphate is induced by inhibition of glucose transport, we examined the activity of glucose uptake by using 2-NBDG, a fluorescently labeled 2-deoxyglucose. Similar to the cell growth, glucose uptake was significantly inhibited by 100 nM TBT, not by 30 nM TBT (Fig. 2B). TA had little effect on glucose uptake. To examine whether the inhibition is regulated by transcription, we tested the effect of short-term exposure. Exposure to TBT for 1 h suppressed glucose uptake (Fig. S1, ESI†), suggesting that gene expression is not involved in the effect of TBT. Since TBT has been shown to activate transcriptional activity of peroxisome proliferator-activated receptor γ (PPARγ),[27,28] we tested the effect of the PPARγ agonist rosiglitazone on the glucose uptake. Treatment with rosiglitazone increased glucose uptake (Fig. S2, ESI†), suggesting that PPARγ is not involved in TBT-induced inhibition of glucose uptake. Furthermore, we examined the activity of hexokinase, which catalyzes the phosphorylation of glucose into glucose-6-phosphate. As shown in Fig. 2C, hexokinase activity was not significantly altered by TBT. Exposure to TA also produced similar results. These data suggest that TBT exposure decreases the amount of glycolytic metabolites *via* inhibition of glucose transport.

AMP-activated protein kinase (AMPK) is known to regulate the translocation of a glucose transporter (GLUT) to the plasma membrane.[29] We examined whether AMPK is involved in the inhibition of glycolytic systems by TBT exposure. Exposure to 100 nM TBT reduced AMPK activity (Fig. 3A). In contrast, TA had little effect on AMPK. In addition, treatment with AICAR (a potent AMPK activator) recovered the inhibitory effect of TBT on glucose uptake (Fig. 3B). To confirm the effect of AICAR, we examined the effect of constitutively active (CA) mutants of AMPK. Similar to the treatment with AICAR, overexpression of CA-AMPK recovered the inhibitory effect of TBT on glucose uptake. Overexpression of dominant-negative mutants of AMPK reduced the basal level of glucose uptake, suggesting that

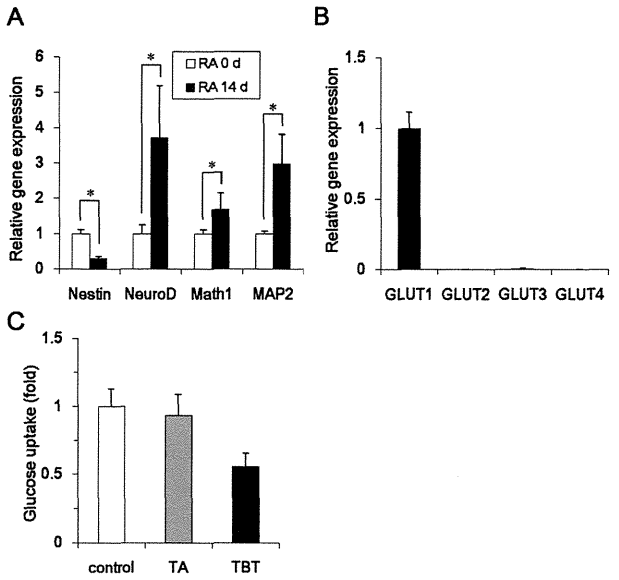

Fig. 5 Effect of neuronal induction on glucose uptake under TBT exposure in NT2/D1 cells. (A) To induce neuronal differentiation, NT2/D1 cells were treated with 10 μM RA for 14 days. The relative expression of neuronal markers (NeuroD, Math1, and MAP2) and a marker of undifferentiation (nestin) were measured by real-time-PCR. The relative changes were normalized to RPL13. (B) Expressions of members of the GLUT family were measured by real-time PCR in differentiated NT2/D1 cells. Relative changes were determined by normalizing to RPL13. (C) After exposure to 100 nM TBT for 24 h, glucose uptake was measured in differentiated cells. The fluorescence intensities of intracellularly incorporated 2-NBDG were measured and normalized to the total cellular protein levels. $^*P < 0.05$.

glucose uptake is AMPK-dependent in NT2/D1 cells. Taken together, these data suggest that TBT exposure suppresses glucose uptake through the inhibition of AMPK activity.

We next examined the mechanism by which AMPK regulates glucose uptake in NT2/D1 cells. Real-time PCR analysis showed that GLUT1 was a major subtype in NT2/D1 cells (Fig. 4A). Since TBT exposure did not affect gene expression of GLUT1 (data not shown), we examined GLUT1 localization by immunohistochemistry. Expression of GLUT1 was observed at the plasma membrane and in the intracellular segment (Fig. 4B). Exposure with TBT reduced the cell surface expression of GLUT1. Treatment with AICAR recovered the inhibitory effect of TBT. To confirm these observations using microscopy, we labeled cell surface-bound GLUT1 by biotinylation of cell surface proteins (Fig. 4C). Using this approach, we determined that TBT exposure reduced the amount of cell surface-bound GLUT1. AICAR reversed this inhibitory effect of TBT. Furthermore, overexpression of GLUT1 partially recovered the TBT-induced inhibition of glucose uptake (Fig. 4D). These data suggest that TBT inhibits glucose uptake mediated by cell surface translocation of GLUT1, a process dependent on AMPK.

To examine whether the effect of TBT was selective for embryonic cells, we used NT2/D1 cells differentiated by retinoic acid.[30] Real-time PCR analysis revealed that RA-treated NT2/D1 cells showed upregulated expression of markers of differentiation (NeuroD, Math1, MAP2) and downregulated expression of a marker of undifferentiation (nestin), confirming the induction of differentiation (Fig. 5A). Real-time PCR confirmed that GLUT1 is a major subtype in the differentiated NT2/D1 cells (Fig. 5B). Furthermore, exposure to 100 nM TBT also reduced glucose uptake in differentiated NT2/D1 cells. In contrast, TA had little effect (Fig. 5C). These data suggest that TBT suppresses glucose uptake in both undifferentiated and differentiated cells.

Discussion

In the present study, we showed that the glycolytic pathway is a novel target of TBT toxicity in human embryonic carcinoma cells. We showed that TBT suppresses AMPK-dependent glucose uptake, and thereby, the amount of glucose-6-phosphate. The inhibitory effects of TBT on glycolytic systems would lead to growth arrest in the cells. Fig. 6 shows a proposed model of TBT-induced toxicity, based on the data observed in our study.

Our studies showed that treatment with 1 μM TBT resulted in the death of human embryonic carcinoma cells (Fig. 1). Consistent with these observations, previous studies have shown that micromolar levels of TBT induce apoptosis in various cells such as human amnion cells,[31] hepatocytes,[32] and neutrophils.[33] In contrast, exposure to 100 nM TBT resulted in neither growth arrest nor cell death. Therefore, we focused on intracellular metabolites as potential mediators of TBT-induced growth arrest. We found that exposure to nanomolar levels of TBT affects the intracellular metabolic balance and decreases the amount of glucose metabolites (Fig. 2). A previous report showed that the organotin compounds such as TBT might be present in human blood at nanomolar levels.[16] Glucose metabolism analysis revealed novel toxic mechanisms

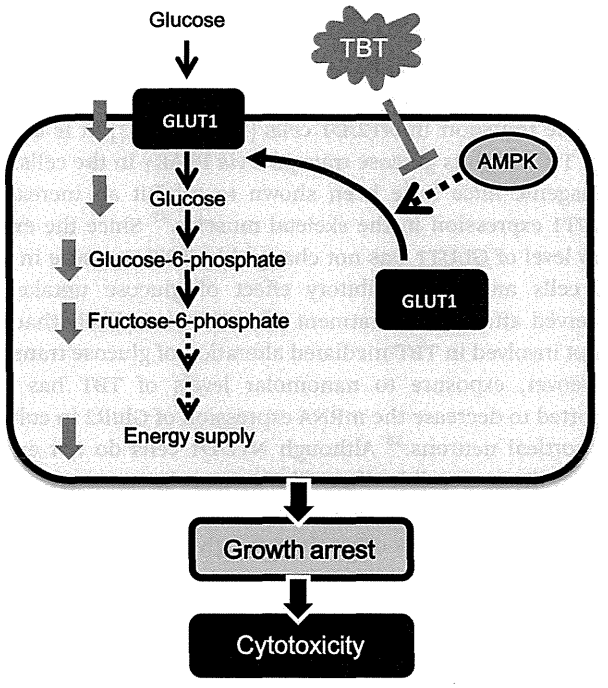

Fig. 6 Proposed model of TBT toxicity in human embryonic carcinoma cells.

for the toxicity of nanomolar levels of TBT. Thus, the glycolytic pathway might account for the unknown toxic mechanism induced by heavy metal exposure.

Our data suggest that the target molecule of TBT toxicity is GLUT1, a major subtype of GLUT in NT2/D1 cells (Fig. 4). Since the expression of GLUT1 is observed in a broad range of cell types, the toxicity of TBT may also be observed in other cells. For example, we showed that TBT reduces glucose uptake in differentiated NT2/D1 cells, which express GLUT1 (Fig. 5). Thus, it is possible that TBT induces toxicity in mature neurons *via* inhibition of GLUT function.

We showed that TBT decreases AMPK activity, one of the GLUT regulators, in NT2/D1 cells (Fig. 3). In addition, overexpression of AMPK or the AMPK activator restored the glucose uptake, confirming that AMPK is a possible target of TBT. In contrast, 500 nM TBT has been shown to increase AMPK phosphorylation in rat cortical neurons.[34] This discrepancy might be due to the concentration of TBT or different types of cells.

Several studies suggest that TBT directly interacts with target enzymes. TBT at a concentration of 10–100 nM has been shown to act as an agonist of PPARγ and the retinoid X receptor (RXR) because of its higher binding affinity compared to intrinsic ligands. Other studies reported that micromolar concentrations of TBT inhibit F1F0 ATP synthase and 11β-hydroxysteroid dehydrogenase by direct interaction.[35,36] Therefore, TBT can bind to multiple targets with broad specificity. It is possible that TBT also interacts with AMPK. On the other hand, calmodulin-dependent protein kinase II (CaMK II) and serine–threonine liver kinase B1 (LKB1) have been shown to phosphorylate AMPK and cause subsequent activation of glucose transport.[29] Furthermore, there may be an additional signaling molecule between TBT and AMPK. It remains to be elucidated how TBT regulates AMPK in embryonic carcinoma cells.

Nanomolar levels of TBT may interact with several targets in other types of cells, such as PPARγ, RXR, and α-amino-3-hydroxy-5-methylisoxazole-4-propionic acid (AMPA) receptors 2 (GluR2). Since rosiglitazone, a PPARγ agonist, increased glucose transport in NT2/D1 cells (Fig. S2, ESI†), it is unlikely that TBT inhibits glucose transport *via* PPARγ in the cells. RXR transgenic mice have been shown to exhibit an increase in GLUT1 expression in the skeletal muscles.[37] Since the expression level of GLUT1 was not changed by TBT exposure in NT2/D1 cells and the inhibitory effect of glucose uptake was observed after a 1 h treatment with TBT, it is likely that RXR is not involved in TBT-mediated alteration of glucose transport. Moreover, exposure to nanomolar levels of TBT has been reported to decrease the mRNA expression of GluR2 in cultured rat cortical neurons.[38] Although NT2/D1 cells do not express GluR2, it is possible that GluR2 may be a target in the differentiated NT2/D1 cells. Further studies are required to examine these targets other than the glycolytic pathway.

Conclusions

We found that exposure to nanomolar levels of TBT mainly targets the glycolytic systems in human embryonic carcinoma cells. Thus, glycolytic systems may be a good target for previously unknown mechanisms of toxicity induced by metal exposure at nanomolar levels.

Conflict of interest

The authors declare that there are no conflicts of interest.

List of abbreviations

AMPK	AMP-activated protein kinase
GLUT	glucose transporter
RA	all-trans retinoic acid
PPARγ	peroxisome proliferator-activated receptor γ
TA	tin acetate
TBT	tributyltin

Acknowledgements

We would like to thank Dr Rathmell and Dr Carling for providing the materials. This study was supported in part by a Health and Labour Sciences Research Grant from the Ministry of Health, Labour and Welfare, Japan (Y. Ka.), a grant from the Program for Promotion of Fundamental Studies in Health Sciences of the National Institute of Biomedical Innovation (NIBIO) (No. 09-02 to Y. Ka.), Grants-in-Aid for Scientific Research (No. 23590322 to Y. Ka. and No. 23310047 to Y. Ko.) from the Japan Society for the Promotion of Science, and a grant from the Smoking Research Foundation (Y. Ka.).

References

1 H. L. Needleman, C. Gunnoe, A. Leviton, R. Reed, H. Peresie, C. Maher and P. Barrett, Deficits in psychologic and classroom performance of children with elevated dentine lead levels, *N. Engl. J. Med.*, 1979, **300**, 689–695.
2 G. Winneke, Developmental aspects of environmental neurotoxicology: lessons from lead and polychlorinated biphenyls, *J. Neurol. Sci.*, 2011, **308**, 9–15.
3 L. G. Costa, M. Aschne, A. Vitalone, T. Syversen and O. P. Soldin, Developmental neuropathology of environmental agents, *Annu. Rev. Pharmacol. Toxicol.*, 2004, **44**, 87–110.
4 J. Dobbing, *Vulnerable periods in developing brain*, in *Appl. Neurochem.*, ed. A. N. Davison and J. Dobbing, Davis, Philadelphia, 1968, pp. 287–316.
5 P. M. Rodier, Developing brain as a target of toxicity, *Environ. Health Perspect.*, 1995, **103**(suppl 6), 73–76.
6 D. Rice and S. Barone Jr, Critical periods of vulnerability for the developing nervous system: evidence from humans and animal models, *Environ. Health Perspect.*, 2000, **108**(suppl 3), 511–533.
7 H. Asakawa, M. Tsunoda, T. Kaido, M. Hosokawa, C. Sugaya, Y. Inoue, Y. Kudo, T. Satoh, H. Katagiri, H. Akita, M. Saji, M. Wakasa, T. Negishi, T. Tashiro and Y. Aizawa, Enhanced

inhibitory effects of TBT chloride on the development of F1 rats, *Arch. Environ. Contam. Toxicol.*, 2010, **58**, 1065–1073.
8 S. Gómez-Ruiz, G. N. Kaluderović, S. Prashar, E. Hey-Hawkins, A. Erić, Z. Zizak and Z. D. Juranić, Study of the cytotoxic activity of di and triphenyltin(IV) carboxylate complexes, *J. Inorg. Biochem.*, 2008, **102**, 2087–2096.
9 L. Rocamora-Reverte, E. Carrasco-García, J. Ceballos-Torres, S. Prashar, G. N. Kaluđerović, J. A. Ferragut and S. Gómez-Ruiz, Study of the anticancer properties of tin(IV) carboxylate complexes on a panel of human tumor cell lines, *ChemMedChem*, 2012, **7**, 301–310.
10 A. González, E. Gómez, A. Cortés-Lozada, S. Hernández, T. Ramírez-Apan and A. Nieto-Camacho, Heptacoordinate tin(IV) compounds derived from pyridine Schiff bases: synthesis, characterization, *in vitro* cytotoxicity, anti-inflammatory and antioxidant activity, *Chem. Pharm. Bull.*, 2009, **57**, 5–15.
11 Y. Kotake, Molecular mechanisms of environmental organotin toxicity in mammals, *Biol. Pharm. Bull.*, 2012, **35**, 1876–1880.
12 T. Noda, S. Morita, T. Yamano, M. Shimizu, T. Nakamura, M. Saitoh and A. Yamada, Teratogenicity study of tri-*n*-butyltin acetate in rats by oral administration, *Toxicol. Lett.*, 1991, **55**, 109–115.
13 A. T. Gardlund, T. Archer, K. Danielsen, B. Danielsson, A. Frederiksson, N. G. Lindquist, H. Lindstrom and J. Luthman, Effects of prenatal exposure to tributyltin and trihexyltin on behavior in rats, *Neurotoxicol. Teratol.*, 1991, **13**, 99–105.
14 Q. Li, M. Osada, K. Takahashi, T. Matsutani and K. Mori, Accumulation and depuration of tributyltin oxide and its effect on the fertilization and embryonic development in the pacific oyster, *Crassostrea gigas*, *Bull. Environ. Contam. Toxicol.*, 1997, **58**, 489–496.
15 Y. Nakatsu, Y. Kotake, K. Komasaka, H. Hakozaki, R. Taguchi, T. Kume, A. Akaike and S. Ohta, Glutamate excitotoxicity is involved in cell death caused by tributyltin in cultured rat cortical neurons, *Toxicol. Sci.*, 2006, **89**, 235–242.
16 M. M. Whalen, B. G. Loganathan and K. Kannan, Immunotoxicity of environmentally relevant concentrations of butyltins on human natural killer cells *in vitro*, *Environ. Res. Lett.*, 1999, **81**, 108–116.
17 L. Pellerin, Food for thought: the importance of glucose and other energy substrates for sustaining brain function under varying levels of activity, *Diabetes Metab.*, 2010, **36**, S59–S63.
18 K. Barnes, J. C. Ingram, O. H. Porras, L. F. Barros, E. R. Hudson, L. G. Fryer, F. Foufelle, D. Carling, D. G. Hardie and S. A. Baldwin, Activation of GLUT1 by metabolic and osmotic stress: potential involvement of AMP-activated protein kinase (AMPK), *J. Cell Sci.*, 2002, **115**, 2433–2442.
19 M. Jing, V. K. Cheruvu and F. Ismail-Beigi, Stimulation of glucose transport in response to activation of distinct AMPK signaling pathways, *Am. J. Physiol.: Cell Physiol.*, 2008, **295**, C1071–C1082.
20 B. Kunievsky, J. Pretsky and E. Yavin, Transient rise of glucose uptake in the fetal rat brain after brief episodes of intrauterine ischemia, *Dev. Neurosci.*, 1994, **16**, 313–320.
21 K. Matsumoto, S. Akazawa, M. Ishibashi, R. A. Trocino, H. Matsuo, H. Yamasaki, Y. Yamaguchi, S. Nagamatsu and S. Nagataki, Abundant expression of GLUT1 and GLUT3 in rat embryo during the early organogenesis period, *Biochem. Biophys. Res. Commun.*, 1995, **209**, 95–102.
22 P. J. Jensen, J. D. Gitlin and M. O. Carayannopoulos, GLUT1 deficiency links nutrient availability and apoptosis during embryonic development, *J. Biol. Chem.*, 2006, **281**, 13382–13387.
23 Y. Kanda and Y. Watanabe, Thrombin-induced glucose transport *via* Src-p38 MAPK pathway in vascular smooth muscle cells, *Br. J. Pharmacol.*, 2005, **146**, 60–67.
24 T. Soga, Y. Ueno, H. Naraoka, Y. Ohashi, M. Tomita and T. Nishioka, Simultaneous determination of anionic intermediates for *Bacillus subtilis* metabolic pathways by capillary electrophoresis electrospray ionization mass spectrometry, *Anal. Chem.*, 2002, **74**, 2233–2239.
25 Y. Kanda and Y. Watanabe, Adrenaline increases glucose transport *via* a Rap1-p38MAPK pathway in rat vascular smooth muscle cells, *Br. J. Pharmacol.*, 2007, **151**, 476–482.
26 N. Hiarta, Y. Sekinoa and Y. Kanda, Nicotine increases cancer stem cell population in MCF-7 cells, *Biochem. Biophys. Res. Commun.*, 2010, **403**, 138–143.
27 T. Kanayama, N. Kobayashi, S. Mamiya, T. Nakanishi and J. Nishikawa, Organotin compounds promote adipocyte differentiation as agonists of the peroxisome proliferator-activated receptor gamma/retinoid X receptor pathway, *Mol. Pharmacol.*, 2005, **67**, 766–774.
28 F. Grün, H. Watanabe, Z. Zamanian, L. Maeda, K. Arima, R. Cubacha, D. M. Gardiner, J. Kanno, T. Iguchi and B. Blumberg, Endocrine-disrupting organotin compounds are potent inducers of adipogenesis in vertebrates, *Mol. Endocrinol.*, 2006, **20**, 2141–2155.
29 D. G. Hardie, F. A. Ross and S. A. Hawley, AMPK: a nutrient and energy sensor that maintains energy homeostasis, *Nat. Rev. Mol. Cell Biol.*, 2012, **13**, 251–262.
30 S. J. Pleasure, C. Page and V. M. Lee, Pure, postmitotic, polarized human neurons derived from NTera 2 cells provide a system for expressing exogenous proteins in terminally differentiated neurons, *J. Neurosci.*, 1992, **12**, 1802–1815.
31 X. Zhu, M. Xing, J. Lou, X. Wang, W. Fu and L. Xu, Apoptotic related biochemical changes in human amnion cells induced by tributyltin, *Toxicology*, 2007, **230**, 45–52.
32 M. Grondin, M. Marion, F. Denizeau and D. A. Averill-Bate, Tributyltin induces apoptotic signaling in hepatocytes through pathways involving the endoplasmic reticulum and mitochondria, *Toxicol. Appl. Pharmacol.*, 2007, **222**, 57–68.
33 V. Lavastre and D. Girard, Tributyltin induces human neutrophil apoptosis and selective degradation of cytoskeletal proteins by caspases, *J. Toxicol. Environ. Health, Part A*, 2002, **65**, 1013–1024.

34 Y. Nakatsu, Y. Kotake, A. Hino and S. Ohta, Activation of AMP-activated protein kinase by tributyltin induces neuronal cell death, *Toxicol. Appl. Pharmacol.*, 2008, **230**, 358–363.
35 C. von Ballmoos, J. Brunner and P. Dimroth, The ion channel of F-ATP synthase is the target of toxic organotin compounds, *Proc. Natl. Acad. Sci. U. S. A.*, 2004, **101**, 11239–11244.
36 A. G. Atanasov, L. G. Nashev, S. Tam, M. E. Baker and A. Odermatt, Organotins disrupt the 11β-hydroxysteroid dehydrogenase type 2-dependent local inactivation of glucocorticoids, *Environ. Health Perspect.*, 2005, **113**, 1600–1606.
37 S. Sugita, Y. Kamei, F. Akaike, T. Suganami, S. Kanai, M. Hattori, Y. Manabe, N. Fujii, T. Takai-Igarashi, M. Tadaishi, J. Oka, H. Aburatani, T. Yamada, H. Katagiri, S. Kakehi, Y. Tamura, H. Kubo, K. N. S. Miura, O. Ezaki and Y. Ogawa, Increased systemic glucose tolerance with increased muscle glucose uptake in transgenic mice overexpressing RXRγ in skeletal muscle, *PLoS One*, **6**, e20467.
38 Y. Nakatsu, Y. Kotake Y, T. Takishit and S. Ohta, Long-term exposure to endogenous levels of tributyltin decreases GluR2 expression and increases neuronal vulnerability to glutamate, *Toxicol. Appl. Pharmacol.*, 2009, **240**, 292–298.

FEBS Open Bio 3 (2013) 387–393

journal homepage: www.elsevier.com/locate/febsopenbio

Identification, expression and characterization of rat isoforms of the serum response factor (SRF) coactivator MKL1☆

Mitsuru Ishikawa[a,1], Jun Shiota[a,1], Yuta Ishibashi[a,1], Tomoyuki Hakamata[a,1], Shizuku Shoji[a], Mamoru Fukuchi[a], Masaaki Tsuda[a], Tomoaki Shirao[b], Yuko Sekino[c], Toshihisa Ohtsuka[d], Jay M. Baraban[e], Akiko Tabuchi[a,*]

[a]Laboratory of Molecular Neurobiology, Graduate School of Medicine and Pharmaceutical Sciences, University of Toyama, 2630 Sugitani, Toyama 930-0194, Japan
[b]Department of Neurobiology and Behavior, Gunma University, Graduate School of Medicine, 3-39-22 Showa-machi, Maebashi 371-8511, Japan
[c]Division of Pharmacology, Biological Safety Research Center, National Institute of Health Sciences, 1-18-1 Kamiyoga, Setagaya-ku, Tokyo 158-8501, Japan
[d]Department of Biochemistry, Graduate School of Medicine/Faculty of Medicine, University of Yamanashi, 1110 Shimokato, Chuo, Yamanashi 409-3898, Japan
[e]Solomon H. Snyder Department of Neuroscience, Johns Hopkins University, School of Medicine, 725 North Wolfe Street, Baltimore, MD 21205, USA

ARTICLE INFO

Article history:
Received 5 June 2013
Received in revised form 21 August 2013
Accepted 4 September 2013

Keywords:
Megakaryoblastic leukemia
Serum response factor
Transcript
Alternative promoter
Transcriptional coactivator

ABSTRACT

Megakaryoblastic leukemia 1 (MKL1) is a member of the MKL family of serum response factor (SRF) coactivators. Here we have identified three rat MKL1 transcripts: two are homologues of mouse MKL1 transcripts, full-length MKL1 (FLMKL1) and basic, SAP, and coiled-coil domains (BSAC), the third is a novel transcript, MKL1-elongated derivative of yield (MELODY). These rat MKL1 transcripts are differentially expressed in a wide variety of tissues with highest levels in testis and brain. During brain development, these transcripts display differential patterns of expression. The FLMKL1 transcript encodes two isoforms that utilize distinct translation start sites. The longer form possesses three actin-binding RPXXXEL (RPEL) motifs and the shorter form, MKL1met only has two RPEL motifs. All four rat MKL1 isoforms, FLMKL1, BSAC, MKL1met and MELODY increased SRF-mediated transcription, but not CREB-mediated transcription. Accordingly, the differential expression of MKL1 isoforms may help fine-tune gene expression during brain development.

1. Introduction

The megakaryoblastic leukemia (MKL) family members, MKL1 and MKL2, function as serum response factor (SRF) coactivators [1–5]. Several studies conducted in non-neuronal cells have shown that MKL1 binds to G-actin via its RPXXXEL (RPEL) motifs and translocates into the nucleus where it binds to and activates SRF in response to actin polymerization and G-actin depletion [6–8]. MKL1 and MKL2 regulate a set of genes that code for cytoskeletal proteins and are involved in alteration of cell shape and motility [5]. MKL family members are also highly expressed in the brain and they regulate morphology of cultured cortical or hippocampal neurons [9–12].

MKL1 isoforms were initially identified in non-neuronal cells. One of the mouse MKL1 cDNAs derived from NIH3T3 cells has two alternative translation start sites; the upstream site uses leucine as the initiator codon and generates full-length MAL/MKL1, MAL/MKL1(fl), while the downstream site employs methionine as the start codon to produce a shorter protein, MAL/MKL1(met) [6]. Another MAL/MKL1 transcript, called BSAC (basic, SAP and coiled-coil domain) has been identified in mouse spleen which contains a 5′-exon different from that of the MAL/MKL1(fl) transcript [2]. Mouse MAL/MKL1 (fl) and MAL/MKL1met are able to translocate from the cytoplasm to the nucleus in response to serum-stimulation in NIH3T3 cells [6]. As MKL1 is expressed prominently in brain and plays a key role in regulating neuronal morphology, we sought to define the pattern of expression of MKL1 transcripts during brain development and whether MKL1 isoforms differ in their ability to regulate SRF-mediated transcription. In the course of these studies, we have identified a novel MKL1 transcript termed MKL1-elongated derivative of yield (MELODY) and two MKL1 transcripts which have homology to mouse MAL/MKL1(fl) and BSAC. Furthermore, we have found that: (1) these MKL1 isoforms are differentially expressed during brain development, and (2) MELODY, in addition to FLMKL1, BSAC and MKL1met, activates SRF-mediated

Abbreviations: BSAC, basic, SAP, and coiled-coil domains; DAPI, 4′, 6-diamidino-2-phenylindole; GFP, green fluorescent protein; MAL, megakaryocytic acute leukemia; MKL1, megakaryoblastic leukemia 1; MELODY, MKL1-elongated derivative of yield; RPEL, arginine proline XXX glutamate leucine; SRF, serum response factor.

[1] These authors equally contributed to this work.

* Corresponding author. Tel.: +81 76 434 7536; fax: +81 76 434 5048.
E-mail address: atabuchi@pha.u-toyama.ac.jp (A. Tabuchi).

2211-5463/$36.00
http://dx.doi.org/10.1016/j.fob.2013.09.001

transcription.

2. Materials and methods

2.1. Animals

Male SD rats for measuring MKL1 mRNA expression were purchased from Sankyo Labo Service Corporation, Inc. (Tokyo, Japan). All experiments were carried out in accordance with the guidelines of the Animal Care and Experimentation Committee of University of Toyama, Sugitani Campus. The protocols were approved as permit numbers (S-2008 PHA-3, S2009 PHA-23, S2010 PHA-1, A2011 PHA-5, A2012 PHA-1). Every effort was made to minimize suffering.

2.2. Cloning of rat MKL1 transcripts

To clone cDNA of rat MKL1 transcripts, the following primers for 5′-rapid amplification cDNA-end (5′-RACE) were initially designed based on the predicted rat MKL1 mRNA sequence (NCBI Reference Sequence: XM_235497.4), which was derived by sequence tagged sites (STS) and expressed sequence tags (EST). The primers correspond to the predicted exons 7 and 8: RT (5′-TCTCATTGAGGTC-3′), sense1 (5′-GAGCCTTCTCTCCAGGCCAA-3′), antisense1 (5′-AGGTCTCTTCCAGAATGTGC-3′), sense2 (5′-GCTGAAGCTGAAGAGAGCCA-3′), antisense2 (5′-CCTGACCAGCTCTGATCTCT-3′). The 5′-RACE procedure was performed by PCR with Pfu DNA polymerase (Promega, Madison, WI, USA), followed by reverse transcription, degradation of RNA, and circularization with 5′-Full RACE Core Set (TaKaRa, Shiga, Japan) in the reaction mixture containing SD rat adult hippocampal RNA. Sequence analysis of the 5′-RACE products revealed that two different 5′-ends were present that are homologous to mouse full length MKL1 and BSAC, respectively. These two fragments were tentatively termed full-length MKL1 (FLMKL1) and basic, SAP and coiled-coil domain (BSAC), respectively. The predicted 1st and 2nd exons were absent in FLMKL1. Thus, the 5′-RACE was further performed with AmpliTaq Gold (Applied Biosystems, Carlsbad, CA, USA), 5′-Full RACE Core Set and primers (RT2: 5′-CCGCTCACTAAGTG-3′; sense3: 5′-GAACTGCAGGAGCTGTCCCT-3′; antisense3: 5′-TTGGCAACAGCTTCGCTCTG-3′; sense4: 5′-TGACTCTGGGCCTCCATCCT-3′; antisense4: 5′-CAGAGACAGGAGCACCGGTT-3′) corresponding to the predicted exon 3. The 5′-RACE product possesses a newly identified 5′-exon and was tentatively named MKL1-elongated derivative of yield (MELODY). To obtain FLMKL1, BSAC and MELODY cDNA including their coding regions, PCR was carried out with rat 7-week hippocampal cDNA as a template, PrimeSTAR Max DNA polymerase (TaKaRa), sense primers (5′-CGGTACCCGGGGATCCTCGCTAGCCACGCTCCCTC-3′ for FLMKL1; 5′-CGGTACCCGGGGATCGCTGGGCTTCCTGTCTGCAC-3′ for BSAC; 5′-CGGTACCCGGGGATCGCAGAGACACCTGTCAGGAC-3′ for MELODY) and antisense primer (5′-CGACTCTAGAGGATCGCCTCTAGGGACTGTGATTGTC-3′ for a common 3′-untranslated region). The sequence analyses of FLMKL1 (DDBJ Accession No. AB588919), BSAC (AB588920) and MELODY (AB588921) were deposited.

2.3. Search of transcription factor-binding sites within rat MKL1 genome

To find transcription factor-binding sites upstream of transcription start site of rat MKL1 isoforms, we used the TF search program (http://mbs.cbrc.jp/research/db/TFSEARCH.html), which is directly owned to the TRANSFAC databases developed at GBF-Braunschweig, Germany [13]. Rat MKL1 genome sequences, shown in the website of Ensembl database (http://www.ensembl.org/index.html), was used for TF search program. One kilobase long upstream of 5′-ends of FLMKL1, MELODY, BSAC were searched at threshold score = 95.0.

2.4. RNA isolation and real-time quantitative PCR

Total RNA was extracted from rat tissues and brain regions using TRIsure (Bioline). Then, RNA was treated with DNase I and further purified using TRIsure again. Using the RNA solution, cDNA was synthesized with SuperScriptII reverse transcriptase (Invitrogen, Carlsbad, CA, USA). In brief, for detection of FLMKL1, BSAC, and MELODY mRNA levels, the PCR was performed in 20 μL of 1× SYBR system using SYBR Green PCR master mix (Applied Biosystems, Foster City, CA, USA) containing 2 μL of cDNA solution and 0.4 μM primers (5′-TCCTTGAGGCTCGGGAGGATA-3′ and 5′-GTCCAGCCCATTCACAGCAATG-3′ for FLMKL1; 5′-GCTTCCTGTCTGCACTCACTC-3′ and 5′-GACGGAGTCCTCACGGAAAC-3′ for BSAC; 5′-CAGAGACACCTGTCAGGACG-3′ and 5′-GTCCAGCCCATTCACAGCAATG-3′ for MELODY). After preheating at 95 °C for 10 min, the samples were denatured at 95 °C for 45 s, annealed at 60 °C for 45 s, and extended at 72 °C for 1 min for 45 cycles. Quantification of each transcript was calculated by the following procedure. In brief, the initial cDNA copy number [DNA_0], which reflects mRNA expression of the sample, was calculated from PCR-amplified cDNA copy number [DNA], Ct value (c), amplification efficiency (e) and cDNA standard curve. The formula, $[DNA] = [DNA_0](1 + e)^c$, was used for calculation.

2.5. Plasmids and antibodies

To generate a series of FLAG-tagged rat MKL1 constructs (FLAG-FLMKL1, FLAG-BSAC, FLAG-MELODY and FLAG-MKL1met), the coding regions of FLMKL1 (from 5′-CCCCCTTCCGTCATT-3′ to 5′-TGGGATTCCTGCTTG-3′), BSAC (from 5′-ACTCTGCTGGAGCCT-3′ to 5′-TGGGATTCCTGCTTG-3′), MELODY (from 5′-GGAGGGGTTACCATC-3′ to 5′-TGGGATTCCTGCTTG-3′) and MKL1met (from 5′-CCGCCTTTGAAAAGT-3′ to 5′-TGGGATTCCTGCTTG-3′) were linked to the downstream (5′-CTTGCGGCCGCGAATTCA-3′) of the FLAG tag sequence of pFLAG-CMV2 vector (SIGMA, St. Louis, MO, USA). The expression vector for enhanced green fluorescent protein (pEGFP-C1) was purchased from Clontech. The SRF reporter vector, 3D.ALuc, generously provided by Dr. R. Treisman (Cancer Research Institute, London, UK) has been described previously [6,9,11]. The CRE-reporter vector, pCRE-Luc (CRE-Luc), and the SRE-reporter vector, pSRE-Luc (SRE-Luc), were purchased from Stratagene (La Jolla, CA, USA). An internal control vector, TK-*Renilla* vector, has been described previously [9]. The following antibodies were used: anti-green fluorescent protein (GFP) made in rabbit (Invitrogen or Medical & Biological Laboratories; 1:500 or 1:1000), anti-FLAG (SIGMA; 1:1000) made in mouse, and anti-α-tubulin (SIGMA; 1:1000) made in mouse.

2.6. Cell culture

NIH3T3 cells were cultured in Dulbecco's modified Eagle medium (DMEM; Invitrogen) containing 10% fetal bovine serum (Invitrogen), 10% Nu-serum (BD Biosciences, San Jose, CA, USA), 2 mM glutamine (Invitrogen), 1% penicillin/streptomycin (Invitrogen), as described previously [9]. For reporter assays, cells were seeded at 5×10^5 cells/well and grown on six-well plates (Nalge Nunc, Naperville, IL, USA).

2.7. Transfection into NIH3T3 cells

Transfection into NIH3T3 cells was performed using lipofectamine (Invitrogen) and Plus reagent (Invitrogen) as described previously [9]. Medium exchange was carried out 4 h after transfection. Cell lysates were prepared 20 h after transfection.

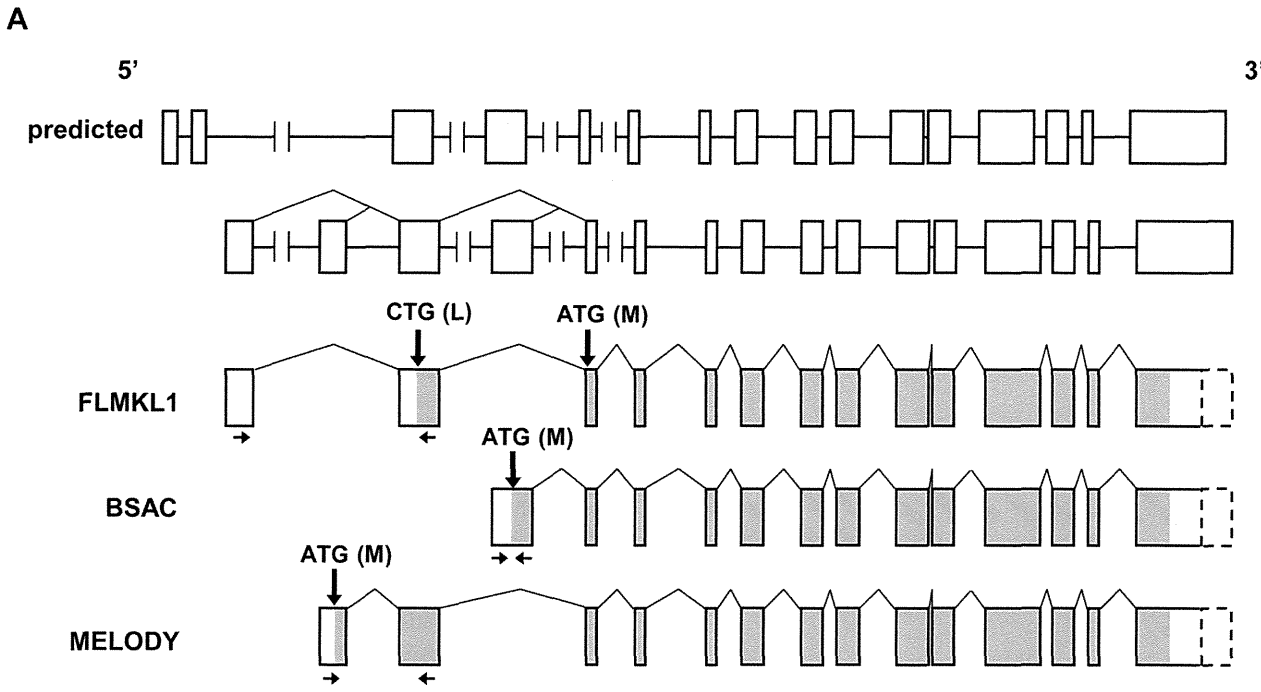

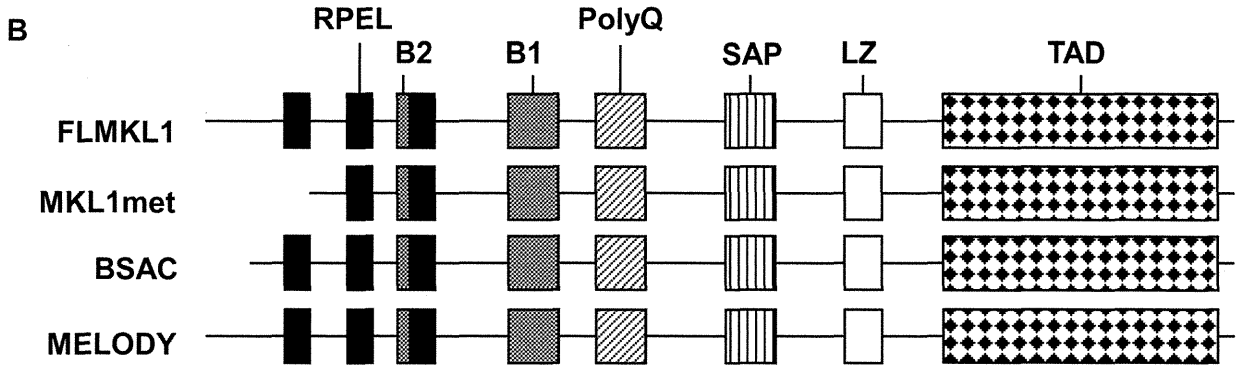

C

```
(FLMKL1)    1:------------------LPPSVIAVNGLDGGGAGENDEEPVLLSLSAAPSPQSEAVANELQELSLQPEL  52
(MKL1met)   0:------------------------------------------------------------------  0
(BSAC)      0:------------------------------------------------------------------  0
(MELODY)    1:MGGVTITKAKVDFSSVVCLPPSVIAVNGLDGGGAGENDEEPVLLSLSAAPSPQSEAVANELQELSLQPEL  70
                                                RPEL
           53:TLGLHPGRNPNLPPLSERKNVLQLKLQQRRTREELVSQGIMPPLKSPAAFHEQRRSLERARTEDYLKRKI 122
            1:--------------------------------------MPPLKSPAAFHEQRRSLERARTEDYLKRKI  30
            1:-----MTLLEPEMLMMAVQSVLQLKLQQRRTREELVSQGIMPPLKSPAAFHEQRRSLERARTEDYLKRKI  65
           71:TLGLHPGRNPNLPPLSERKNVLQLKLQQRRTREELVSQGIMPPLKSPAAFHEQRRSLERARTEDYLKRKI 140
```

Fig. 1. Deduced exon–intron organization and domain structure of rat MKL1 isoforms. (A) Deduced exon–intron organization. Boxes indicate exons. Sizes of exons and introns are depicted approximately to scale. The predicted exon locations (on the top) are illustrated in accordance with the NCBI's information (NCBI Reference Sequence: XM_235497.4 and NW_047780.1). The exon (open boxes)–intron organization (the second from the top) is illustrated based on the sequence data shown in this study. The last three structures indicate the deduced exon–intron organization of FLMKL1, BSAC and MELODY variants, respectively. Shaded regions indicate the open reading frames. Boxes drawn by broken lines indicate the predicted 3′-untranslated regions, which were not analyzed in this study. Thick arrows indicate the putative initiation codons. Thin arrows indicate the location of primers used for real-time quantitative PCR measurements of each mRNA transcript. The FLMKL1 possesses two putative initiation codons, possibly giving rise to two different proteins, FLMKL1 and MKL1met, respectively (also shown in Fig. 1B). (B) Conserved motifs of FLMKL1, MKL1met, BSAC and MELODY. The illustrated domains were predicted on the basis of Pfam (http://www.sanger.ac.uk/). FLMKL1 and MKL1met can be produced by the distinct usage of two initiation codons, CTG and ATG, in a common transcript, respectively (see (A)). RPEL: arginine proline XXX glutamate leucine; B1 and B2: basic regions 1 and 2; PolyQ: polyglutamine repeat; SAP: SAF-A/B, Acinus and PIAS; LZ: leucine zipper; TAD: transcriptional activation domain. (C) Variation of the N-termini of FLMKL1, MKL1met, BSAC and MELODY. The numbers at both ends indicate the amino acid position of each isoform. The rectangle indicates the first RPEL motif. The first amino acids of the RPEL motif are written in white.

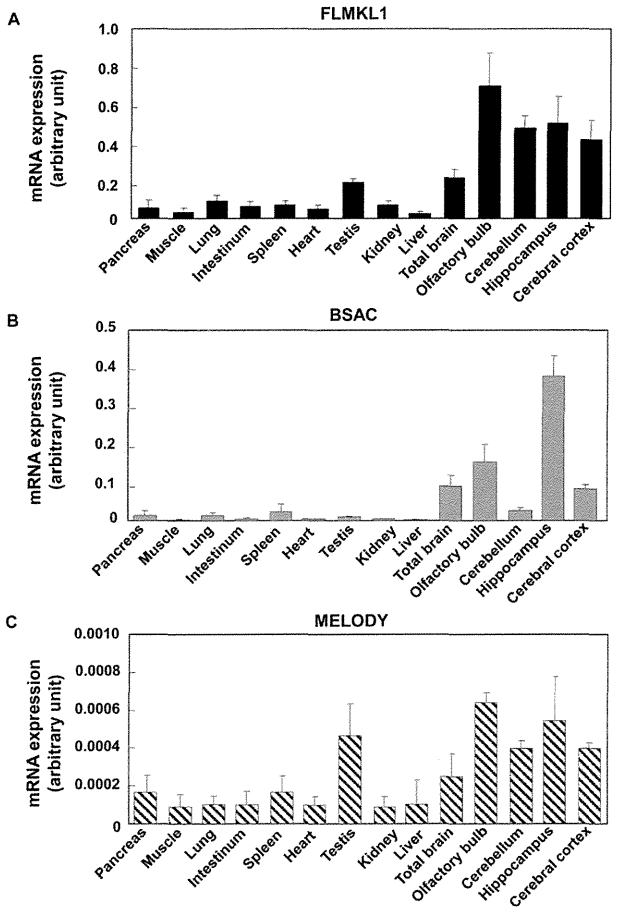

Fig. 2. Regional expression of rat MKL1 transcripts in adult tissues. Complementary DNA derived from several tissues of 7-week old rat (pancreas, muscle, lung, intestinum, spleen, heart, testis, kidney, liver, total brain, olfactory bulb, cerebellum, hippocampus and cerebral cortex) was subjected to real-time quantitative PCR analysis with FLMKL1 (A), BSAC (B), MELODY (C) specific primers. Primer positions are illustrated in Fig. 1A. Data represent the means ± SD from at least three independent experiments.

2.8. Western blotting

In order to measure the expression levels of FLAG-tagged rat MKL1 variants, we performed Western blotting for the FLAG tag (Fig. 4A). Protein was extracted in the whole cell extract buffer containing 25 mM HEPES, 0.3 M NaCl, 1.5 mM $MgCl_2$, 0.2 mM EDTA, 0.1% Triton X-100, 20 mM β-glycerophosphate, 10 μg/mL aprotinin, 10 μg/mL leupeptin, 1 mM sodium orthovanadate, 1 mM dithiothreitol, and 1 mM phenylmethylsulfonyl fluoride. After centrifugation, the cell lysates were mixed with an equal volume of 2 × Laemmli sample buffer (Bio-Rad Laboratories, Hercules, CA, USA) and subjected to sodium dodecyl sulfate–polyacrylamide gel electrophoresis. Protein detection was carried out with the enhanced chemiluminescence (ECL) protocol (GE Healthcare, Little Chalfont, UK).

2.9. Reporter assay

Transcriptional activity was monitored using either the firefly luciferase or *Renilla* luciferase activity as described previously [9]. Luciferase activity was monitored using dual luciferase assays according to the manufacturer's instructions (Promega).

2.10. Statistical analysis

Statistical significance of treatment effects was analyzed by ANOVA.

3. Results

3.1. Identification of rat MKL1 transcripts

To identify rat MKL1 transcripts, we first designed primers for 5′-rapid amplification cDNA-end (5′-RACE) based on the predicted rat MKL1 mRNA sequence (NCBI Reference Sequence: XM_235497.4) (Fig. 1A, on the top). Sequence analysis of the 5′-RACE products generated from primers located in predicted exons 7 and 8 revealed that two different 5′-ends were present that were homologous to mouse full length MAL/MKL1 and BSAC. However, since the predicted exons 1 and 2, which were provided by NCBI reference sequence, were absent from the presumed 5′ fragment of rat FLMKL1, we performed another round of 5′-RACE with primers corresponding to the predicted exon 3. Although these 5′-RACE products still did not contain sequences corresponding to either of the predicted exons 1 and 2, which were provided by NCBI reference sequence, they did contain a transcript with a novel 5′ exon that we refer to as MELODY (MKL1-elongated derivative of yield). Subsequent cloning and sequence analysis of the entire FLMKL1 (DDBJ: AB588919), BSAC (DDBJ: AB588920) and MELODY (DDBJ: AB588921) cDNAs revealed that the predicted 1st and 2nd exons were absent from all three rat MKL1 cDNA obtained in this study (Fig. 1A). Each of the three rat MKL1 transcripts identified have distinct 5′-exons, implying that alternative promoters may be located upstream of each of these 5′-exons. To find transcription factor-binding sites of rat MKL1 gene, we used TF search [13]. Binding sites of ETS, AML-1a are located within 1 kbp upstream of 5′ ends of FLMKL1. Binding sites of SRY, CdxA, Nkx-2 are located within 1 kbp upstream of 5′ ends of MELODY. SRY, CdxA are located within 1 kbp upstream of 5′ ends of BSAC cDNA. These binding sites may be involved in differential regulation of MKL1 isoform transcription.

The study by Miralles et al. demonstrated that mouse FLMKL1 contains two alternative translation start sites [6]. The two translation products generated, FLMKL1 and MKL1met, possess three and two RPEL motifs, respectively (Fig. 1B, on the top and the second rows). Although the junction between the distinct 5′ exon located in BSAC and the first exon shared in common by all the transcripts is located at the N-terminal border of the first RPEL domain, we noted that amino acid sequences of this domain is identical in BSAC, FLMKL1 and MELODY, except for the very first amino acid residue which is switched to serine in BSAC instead of asparagine present in FLMKL1 and MELODY (Fig. 1C). The nucleotide and amino acid sequences of rat MKL1 transcripts identified here are summarized in supporting information figures available online (Figs. S1, S2 and S3). In comparing these cDNA nucleotide sequences with the corresponding rat genomic sequence (NCBI Reference Sequence: NW_047780.1 and NW_001084859.1), we noted a discrepancy in one nucleotide (the 2816th base in FLMKL1 (DDBJ: AB588919), the 2671st base in BSAC (DDBJ: AB588920) and the 2798th base in MELODY (DDBJ: AB588921) (Figs. S1, S2 and S3). All three cDNA sequences contain T residues rather than a C residue reported in the genomic database, a substitution that would result in a switch from serine to leucine. It is still unknown whether or not this conversion is due to RNA editing or a single nucleotide polymorphism.

3.2. Tissue-distribution of rat MKL1 transcripts

We next examined the tissue-distribution of FLMKL1, BSAC, and MELODY mRNAs. Specific primers were designed for the detection of FLMKL1, BSAC and MELODY expression as shown in Fig. 1A (arrows). Initially, we confirmed whether quantitative PCR analysis could detect the mRNA expression of each transcript specifically. No PCR-amplification was observed in the reverse transcription-free samples (Fig. S4, control−), but bands appeared when each transcript-carrying plasmid template (Fig. S4, control+) or reverse transcribed samples (Fig. S4, 14 kinds of tissues) were used. This showed that PCR products

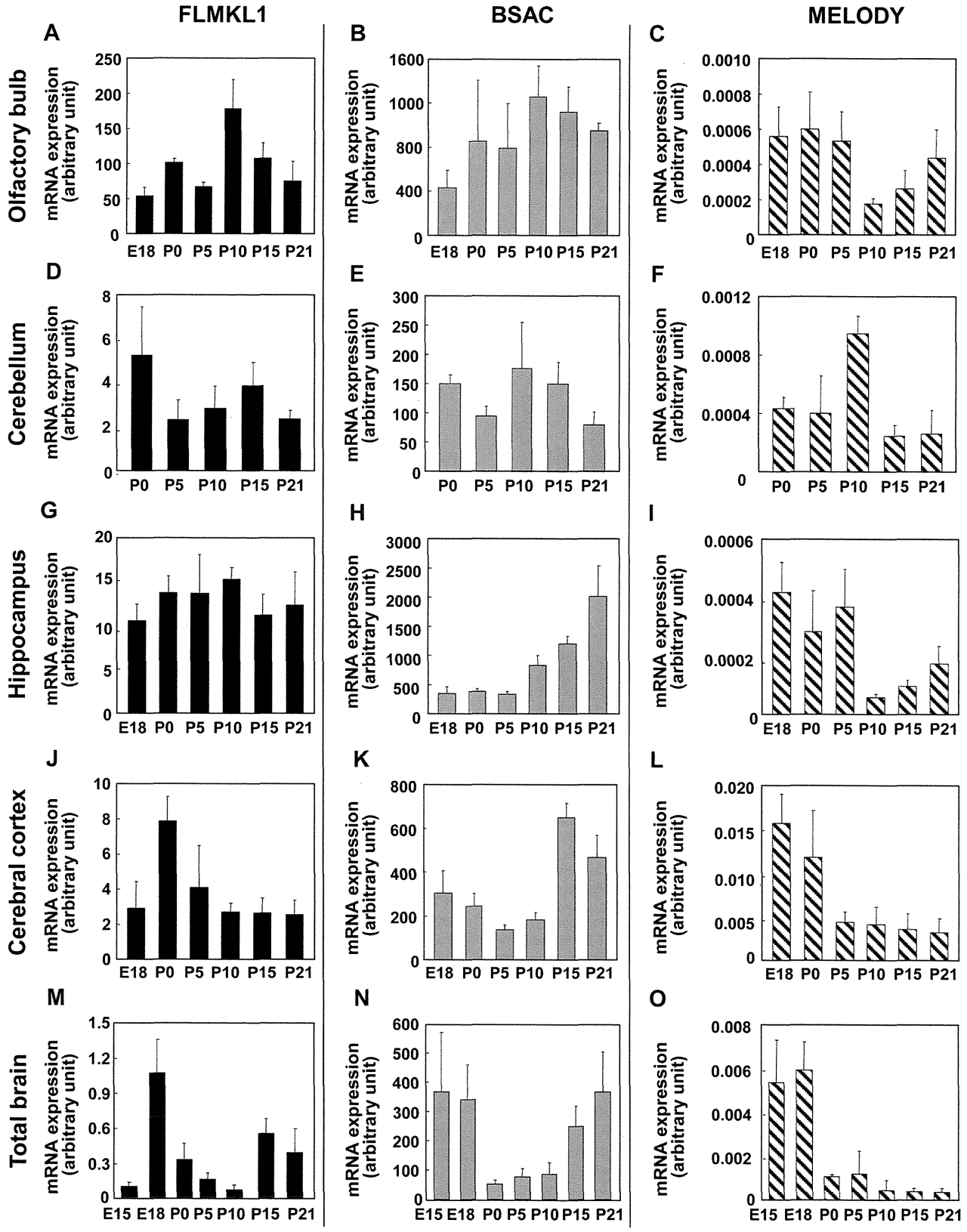

Fig. 3. Differential expression of rat MKL1 transcripts in the developing brain. Samples were prepared from the olfactory bulb (A–C), cerebellum (D–F), hippocampus (G–I), cerebral cortex (J–L) and total brain (M–O) and subjected to real-time quantitative PCR analysis with FLMKL1 (A, D, G, J and M), BSAC (B, E, H, K and N) and MELODY (C, F, I, L and O) specific primers. E15, embryonic day 15; E18, embryonic day 18; P0, post-natal day 0 (day of birth); P5, post-natal day 5; P10, post-natal day 10; P15, post-natal day 15, P21; post-natal day 21. Bar graphs represent the means ± SD from at least three independent experiments.